

Dispersive optical model description of nucleon scattering on Pb–Bi isotopes

Xiuniao Zhao,¹ Weili Sun,² R. Capote,³ E.Sh. Soukhovitskiĭ & D.S. Martyanov,⁴ and J.M. Quesada⁵

¹Graduate School of China Academy of Engineering Physics, Beijing 100088, China

²Institute of Applied Physics and Computational Mathematics, Beijing 100094, China*

³NAPC–Nuclear Data Section, International Atomic Energy Agency, Vienna A-1400, Austria†

⁴Joint Institute for Energy and Nuclear Research, Minsk-Sosny 220109, Belarus

⁵Departamento de Física Atómica, Molecular y Nuclear,
Universidad de Sevilla, Apartado 1065, Sevilla E-41080, Spain

A recently derived dispersive optical model potential (DOMP) for ²⁰⁸Pb is extended to consider the non-locality in the real potential and the shell-gap in the definition of the nuclear imaginary potentials near the Fermi energy. The modified DOMP improves the simultaneous description of nucleon scattering on ²⁰⁸Pb and of the ²⁰⁸Pb particle-hole bound states. The new potential is shown to give a very good description of nucleon scattering data on near-magic targets ^{206,207}Pb and ²⁰⁹Bi.

PACS numbers: 24.10.Ht, 24.10.Dr, 21.10.Pc

I. INTRODUCTION

A unified description of scattering and bound single-particle states can be achieved by using dispersive optical model potentials (DOMP), *e.g.*, see an excellent review paper recently written by Dickhoff and Charity [1] and references therein. As pointed out in the review, special attention deserves the empirical DOMP, where the dispersive contribution $\Delta V(E)$ to the mean field is calculated using a dispersion relation that follow from the requirement of causality. The dispersive potential can be viewed as the “dynamic part” of the mass operator in shell model, which is an extension of the optical model to encompass both positive and negative energies [2, 3]. Using DOMP, the description of bound and scattering states can be simultaneously achieved by using the same nuclear mean field.

Phenomenological DOMP following the Lane formulation have been developed by authors [4–10] and mostly applied to describe nucleon scattering on well deformed target nuclei using a coupled-channel formalism. Those potentials very accurately describe available experimental data of nucleon scattering from keV up to 150–200 MeV of incident nucleon energy. However, deformed nuclei do not have bound-state experimental data available as the bound states are very fragmented due to the deformation.

The analysis of neutron bound states of ²⁰⁸Pb by DOMP [10, 11] was recently undertaken to test at negative energies the derived DOMP using our methodology; calculated DOMP energies of the particle-hole bound states were compared to other calculated values [12, 13] as well as to the existing experimental data [14]. Some inconsistencies in the data description were found in Ref. [11] including problems to describe accurately the total cross sections in the region from 5 up to 10 MeV

and, at the same time, achieve a nice description of the bound-state data.

In this work, the non-locality of the real potential is considered, and the shell-gap in magic nuclei is used to modify the imaginary potentials near the Fermi energy. The impact of the improved physical model on our ability to describe simultaneously the scattering and bound-state data of lead and bismuth isotopes is studied below.

II. DISPERSIVE SPHERICAL OPTICAL MODEL POTENTIAL

A dispersive optical model is defined by energy-dependent real V_i ($i = HF, v, s, C, so$) and imaginary W_i ($i = v, s, so$) functionals for the so-called “Hartree-Fock” (HF), volume (v), surface (s), Coulomb (C) and spin-orbit (so) potentials, respectively and also by the corresponding dispersive contributions to the real potential ΔV_v , ΔV_s , and ΔV_{so} which are calculated analytically from the corresponding imaginary potentials [9, 15, 16]. The general formulation of the Lane-consistent spherical dispersive optical potential has been published previously (*e.g.*, see Eqs.(1)–(3) in Ref. [11]), and is not repeated here.

It is well known (see *e.g.*, Ref. [1]) that the real mean-field potential $V_{HF}(\mathbf{r}, \mathbf{r}')$ is non-local and energy independent. A parametrization of such nonlocal potential was postulated by Perey and Buck to be of Gaussian type [17]:

$$V_{HF}(\mathbf{r}, \mathbf{r}') = \mathbf{V}(\mathbf{r}) \exp(-|\mathbf{r} - \mathbf{r}'|^2/\beta^2), \quad (1)$$

where the parameter β is a non-locality range given in fermi. The local energy approximation of such non-local potential [17] then results in the following implicit equation:

$$V_{HF}(E) = A_{HF} \exp\left(-\frac{\mu\beta^2}{(\hbar c)^2}[E + V_{HF}(E)]\right). \quad (2)$$

Note that both A_{HF} and the potential $V_{HF}(E)$ in Eq. (2) are assumed to be positive. To obtain the potential depth

* sun_weili@iapcm.ac.cn

† r.capotenoy@iaea.org

TABLE I. Dispersive optical-model potential parameters for nucleon induced reactions on lead and bismuth isotopes.

	Volume	Surface	Spin-orbit	Coulomb
Real Potential	$V_0=81.5+0.0292(A-208)$ MeV $\beta=0.912$ fm $C_{\text{viso}}=29.35$ MeV	dispersive	$V_{\text{so}}=7.61$ MeV $\lambda_{\text{so}}=0.006$ MeV $^{-1}$	$C_{\text{Coul}}=1.288$ MeV
Imaginary Potential	$A_v=12.81$ MeV $B_v=65.56$ MeV $E_a=56$ MeV $\alpha = 0.12$ MeV $^{1/2}$	$W_0=19.66$ MeV $B_s=8.99$ MeV $C_s=0.025$ MeV $^{-1}$ $C_{\text{wiso}}=50.71$ MeV	$W_{\text{so}}=-3.1$ MeV $B_{\text{so}}=160$ MeV	
Potential Geometry (fm)	$r_{\text{HF}}=1.226-0.00176(A-208)$ $a_{\text{HF}}=0.647+0.002417(A-208)$ $r_v=1.321$ $a_v=0.6267-0.00658(A-208)$	$r_s=1.1858+0.03418(A-208)$ $a_s=0.6195$	$r_{\text{so}}=1.194$ $a_{\text{so}}=0.6426$	$r_c=1.27$ $a_c=0.671$

TABLE II. The average particle (hole) single-particle energies E_P^i ($i = n, p$) in MeV for nucleon induced reaction on selected targets.

	^{206}Pb	^{207}Pb	^{208}Pb	^{209}Bi
E_P^n	-6.75	-6.74	-3.95	-4.62
E_P^p	-3.57	-3.72	-3.81	-3.81

$V_{\text{HF}}(E)$ at a given energy E it is necessary to solve the Eq. (2) by iterations¹. Note that both A_{HF} and β are independent of iterations on V_{HF} for a given energy E . The reduced mass μ in the formula is calculated using relativistic kinematics and, therefore, is also a function of the incident nucleon energy E . The isospin dependence of the potential (the Lane term [18, 19]) was considered in real $V_{\text{HF}}(E)$ and imaginary surface $W_s(E)$ potentials as follow,

$$A_{\text{HF}} = V_0 \left[1 + (-1)^{Z'+1} \frac{C_{\text{viso}}}{V_0} \frac{N-Z}{A} \right] \quad (3)$$

$$A_s = W_0 \left[1 + (-1)^{Z'+1} \frac{C_{\text{wiso}}}{W_0} \frac{N-Z}{A} \right] \quad (4)$$

where V_0 , C_{viso} , W_0 and C_{wiso} are undetermined constants. Many authors found that the imaginary volume potential does not depend on the isospin. The isospin constants C_{viso} and C_{wiso} should be determined mainly using quasi-elastic (p,n) scattering data.

The energy dependencies for the imaginary volume term W_v , the imaginary surface term W_s and the spin-orbit imaginary term W_{so} are taken as the ones suggested by Brown and Rho [20], Delaroche *et al.* [21] and Koning *et al.* [22], respectively. In this work, following Mahaux *et al.* [23] and Molina *et al.* [24], a modified definition for the imaginary part of the OMP is taken as follows:

$$W_v(E) = \begin{cases} 0 & E_F < E < E_P \\ A_v \frac{(E-E_P)^2}{(E-E_P)^2 + (B_v)^2} & E > E_P \end{cases} \quad (5)$$

¹ Solution of Eq. (2) can be expressed explicitly through the special function Lambert W (*a.k.a.*, product logarithm) as:

$$V_{\text{HF}}(E) = \frac{W[A_{\text{HF}} \exp(-\lambda E)]}{\lambda}, \text{ where } \lambda \equiv \frac{\mu\beta^2}{(\hbar c)^2}.$$

$$W_s(E) = \begin{cases} 0 & E_F < E < E_P \\ A_s \frac{(E-E_P)^2}{(E-E_P)^2 + (B_s)^2} \times \exp(-C_s|E-E_P|) & E > E_P \end{cases} \quad (6)$$

$$W_{\text{so}}(E) = \begin{cases} 0 & E_F < E < E_P \\ W_{\text{so}} \frac{(E-E_P)^2}{(E-E_P)^2 + (B_{\text{so}})^2} & E > E_P \end{cases} \quad (7)$$

The imaginary part of the DOM potential is assumed to be zero inside the shell gap Δ , which is related to the average energy of the single-particle (-hole) states E_P as $\Delta = 2(E_P - E_F)$. Obviously, if there are no states in the shell-gap we have to set the absorption to zero. Both E_P and E_F are different for neutron and proton induced reactions. For nuclei far from magic E_P is approximately equal E_F , therefore the shell-gap is zero and can be neglected. The symmetry condition $W(2E_F - E) = W(E)$ is used to extend the imaginary part of the OMPs for energies below the Fermi energy. This analytical extension is needed for the calculation of the dispersive corrections.

It should be noted that the DOM analysis of neutron scattering on ^{27}Al [24] showed the importance of the dispersive contribution to describe $\sigma_T(E)$ data for energies above 100 MeV using a non-symmetric version of the volume absorptive potential for large positive and large negative energies as proposed by Mahaux and Sartor [23, 25]. Similar behavior was confirmed in many subsequent analysis of DOMP's derived on different targets [4–10]. Following Mahaux and Sartor [25], the assumption that the imaginary potential $W_v(E)$ is symmetric about $E = E_F$ (according to equation $W(2E_F - E) = W(E)$) is modified above some fixed energy E_a , which is expected to be close to 60 MeV, but it is treated as a parameter.

Optical model code OPTMAN [26–28] that includes the calculation of (p,n) quasi-elastic scattering [29] was used for cross-section calculations for positive energies. The parameters of the dispersive optical model potential were searched for by minimizing the quantity χ^2 in the usual way [30]. All experimental data used in the fitting process are taken from the EXFOR database [31] and is exactly the same database used to derive the DOMP's

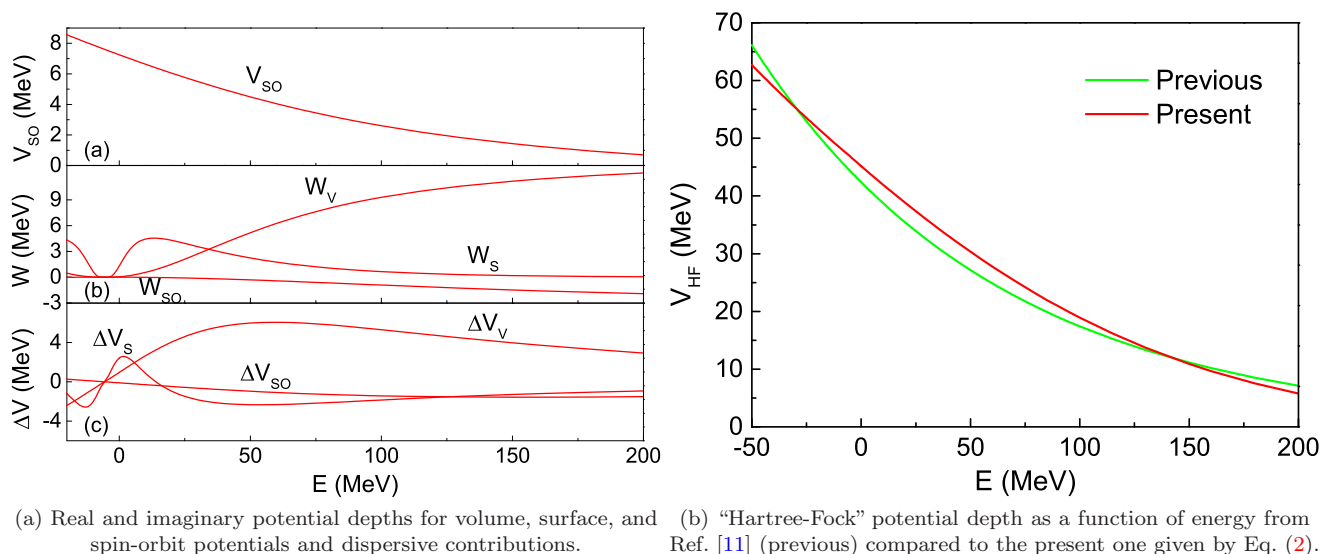


FIG. 1. DOMP depths and dispersive contributions as a function of E for the $n+^{208}\text{Pb}$ reaction between -50 and 200 MeV.

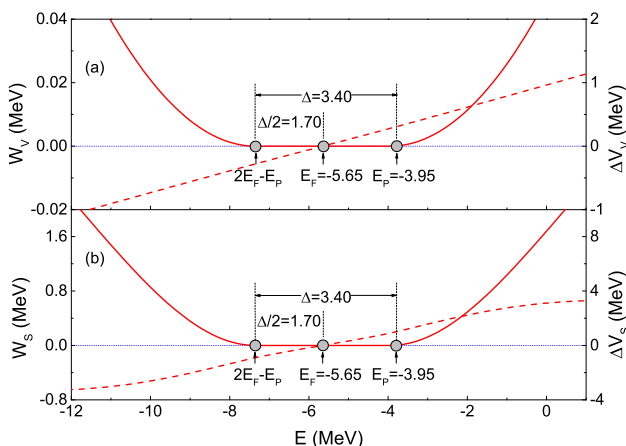


FIG. 2. Energy dependence of the depths of volume, surface imaginary potential (solid curve) and dispersion correction terms (dashed curve) near the Fermi energy E_F calculated for the $n+^{208}\text{Pb}$ reaction. The effect of the assumed shell-gap $2\Delta = 2(E_F - E_P) = 3.4$ MeV on the imaginary potentials is clearly seen.

describing scattering on ^{208}Pb target and published in Refs. [10, 11].

Additionally, the calculation of ^{208}Pb bound states that depends on the real potential [11] is also used in the DOMP optimization using the experimental data quoted in Ref. [14]. Newly derived DOMP parameters are listed in Table I and corresponding average particle (hole) energies E_P^n and E_P^p that define the imaginary potentials are listed in Table II.

Figure 1(a) shows the obtained energy dependence of the real spin-orbit potential, of the imaginary (absorptive) potentials, and of the corresponding dispersive correction terms near the Fermi energy for the $n+^{208}\text{Pb}$ reaction. A comparison of the energy dependence of the ‘‘Hartree-Fock’’ V_{HF} potential is shown in Fig. 1(b). ‘‘Previous’’ refers to the V_{HF} potential from Ref. [11]

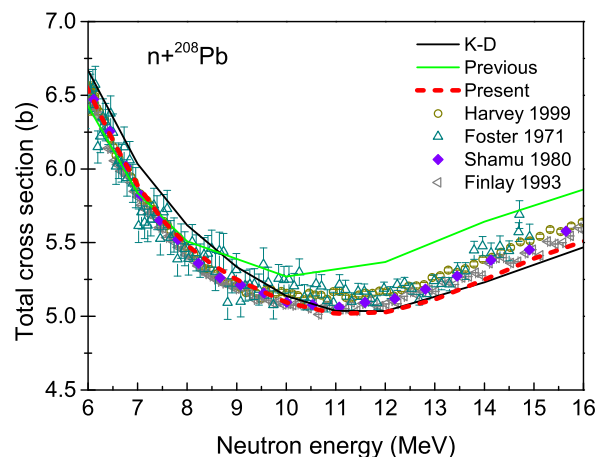


FIG. 3. Comparison of the calculated total cross section for the $n+^{208}\text{Pb}$ reaction with measurements. Calculations using the Koning-Delaroche [22], the DOMP from our previous work [11], and the current DOMP are shown. Experimental data are taken from EXFOR [31], Refs. [32–35].

which is compared to the local approximation of the non-local potential used in this work (see Eq. (2) labelled as ‘‘Present’’).

The depth of new ‘‘Hartree-Fock’’ V_{HF} potential given by Eq. (2) is lower below the Fermi energy, falls more slowly up to 100 MeV and decreases faster above that energy as compared to the exponentially decreasing potential used in Ref. [11]. A shallower potential well given by the Perey-Buck non-local approximation [17] proved to improve the description of the bound-state as well as scattering data as will be shown below.

Figure 2 zooms on the energy dependence of the imaginary (absorptive) potentials and corresponding dispersive-correction terms near the Fermi energy for the $n+^{208}\text{Pb}$ system. The figure clearly shows that the imaginary potentials vanish from the energy $(2E_F - E_P)$ up to the energy E_P reflecting the shell gap. However, the

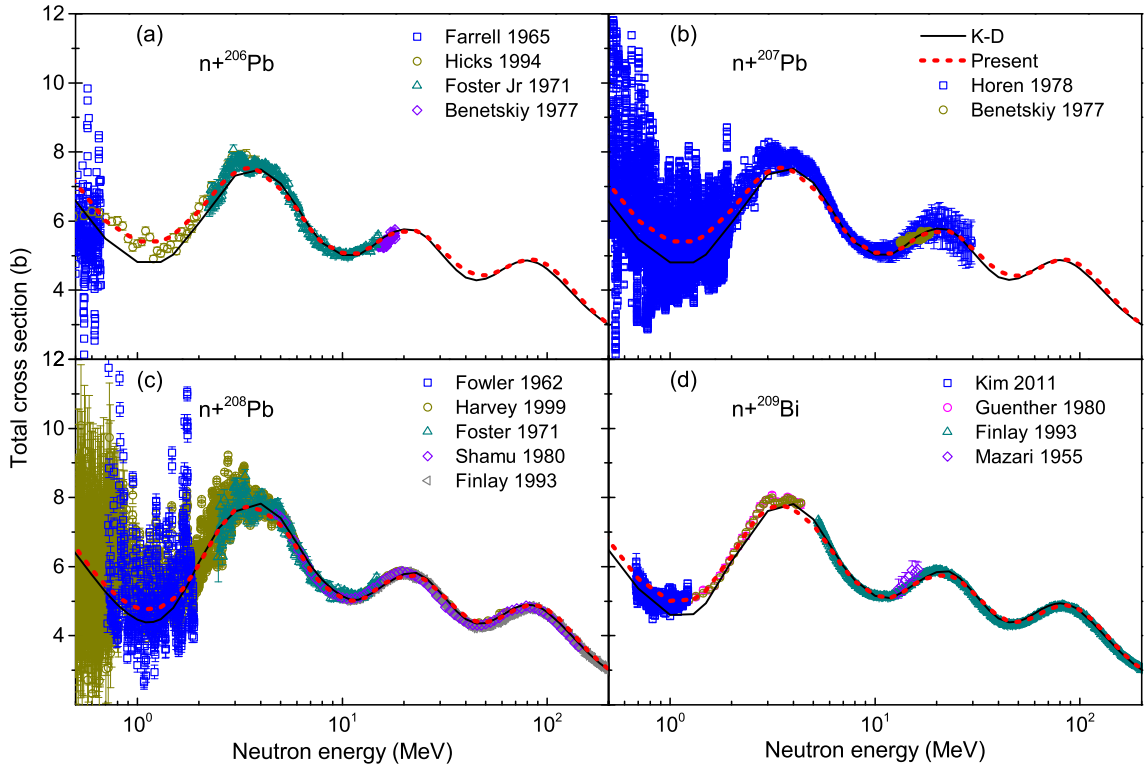


FIG. 4. Comparison of total cross section for $n+^{206}\text{Pb}$, ^{207}Pb , ^{208}Pb and ^{209}Bi reactions with measurements, as well as the results of Koning-Delaroche calculations[22]. Experimental data are taken from Refs. [32–43].

dispersive correction remains non-zero in that region as discussed in Refs. [15, 16].

III. RESULTS AND DISCUSSION

The calculation of neutron total cross section for the ^{208}Pb target using our new DOMP is compared with the results of Koning-Delaroche [22] and our previously derived DOMP [11] in Fig. 3 in the energy range from 6 up to 16 MeV. The potential from Ref. [11] was worse than Koning-Delaroche description [22] in this region. Results from the current work shows a clear improvement over our previous work, the new DOMP results are in good agreement with data as well as with Koning-Delaroche potential calculations in this energy region.

The calculation of neutron total cross sections for ^{206}Pb , ^{207}Pb , ^{208}Pb and ^{209}Bi are compared in Fig. 4 with the results of Koning-Delaroche potential [22] from 500 keV up to 200 MeV of incident neutron energy. The calculated total cross section using the new DOMP is in fair agreement with Koning-Delaroche results above 5 MeV, but reproduces better the experimental data below that energy for all targets.

The real part of our derived DOM potential is the shell model potential, and can be used to calculate the energies of the bound single-particle states of the magic nuclei ^{208}Pb . This potential includes the sum of the Hartree-Fock term $V_{HF}(E_{nlj})$, the real spin-

orbit term $V_{SO}(E_{nlj})$, and all dispersive correction terms $\Delta V_v(E_{nlj})$, $\Delta V_s(E_{nlj})$ and $\Delta V_{so}(E_{nlj})$ with the corresponding geometry-form-factors.

The experimental values of the neutron single-particle energies of the various single-particle and hole states for ^{208}Pb were taken from Ref. [14]. The predicted single particle (hole) energies are compared with the experimental data in Fig. 5. Results labelled “DOM(MR)” and “DOM(MR+35%)” represent the Morillon and Romain calculations from Ref. [13]; the label “ $DOM_{previous}$ ” corresponds to calculations from our previous publication [11], and the label “ $DOM_{present}$ ” represents the current work. The description of the single particle bound states is significantly improved compared to Ref. [13], and slight improvement can be seen relative to our previous work.

The neutron single-particle energies for last single-particle state and first single-hole state were calculated for the ^{208}Pb target; the absolute values of these two energies define the neutron separation energies $S_n(A)$ and $S_n(A+1)$. The calculated values of $S_n(A)$ and $S_n(A+1)$ are 7.47 MeV and 3.85 MeV, respectively. These results are in excellent agreement with the corresponding experimental data 7.37 MeV and 3.94 MeV [44, 45]. The root mean square(rms) radii for each orbit and single particle densities were also calculated and the agreement with results from Ref. [14] is similar to what we already published for ^{208}Pb [11].

Figure 6 shows calculated elastic scattering angular distributions of neutrons and protons incident on ^{206}Pb ,

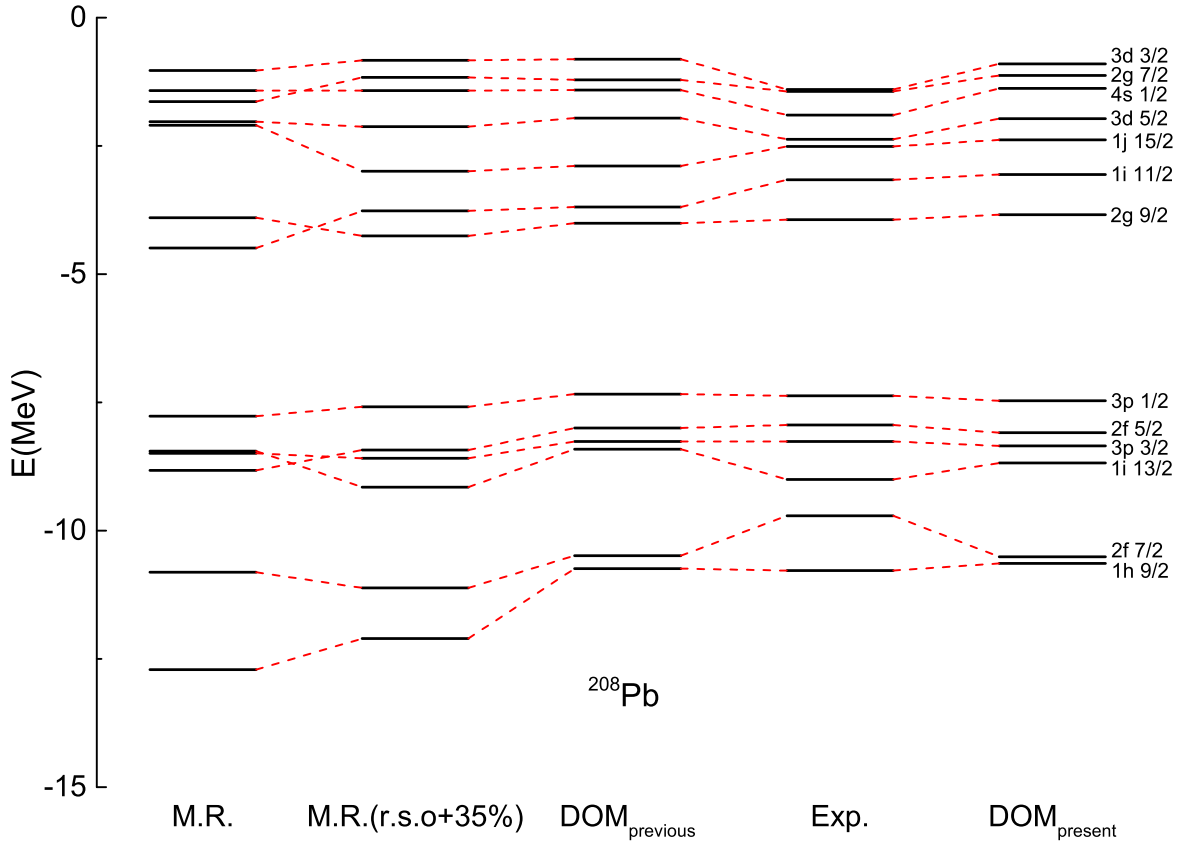


FIG. 5. Neutron single-particle (hole) energies in ^{208}Pb , the first and second columns display the results from Ref. [13], the third column – Ref. [11], the fifth column – current work. In the fourth column the experimental values taken from Ref. [14] are shown.

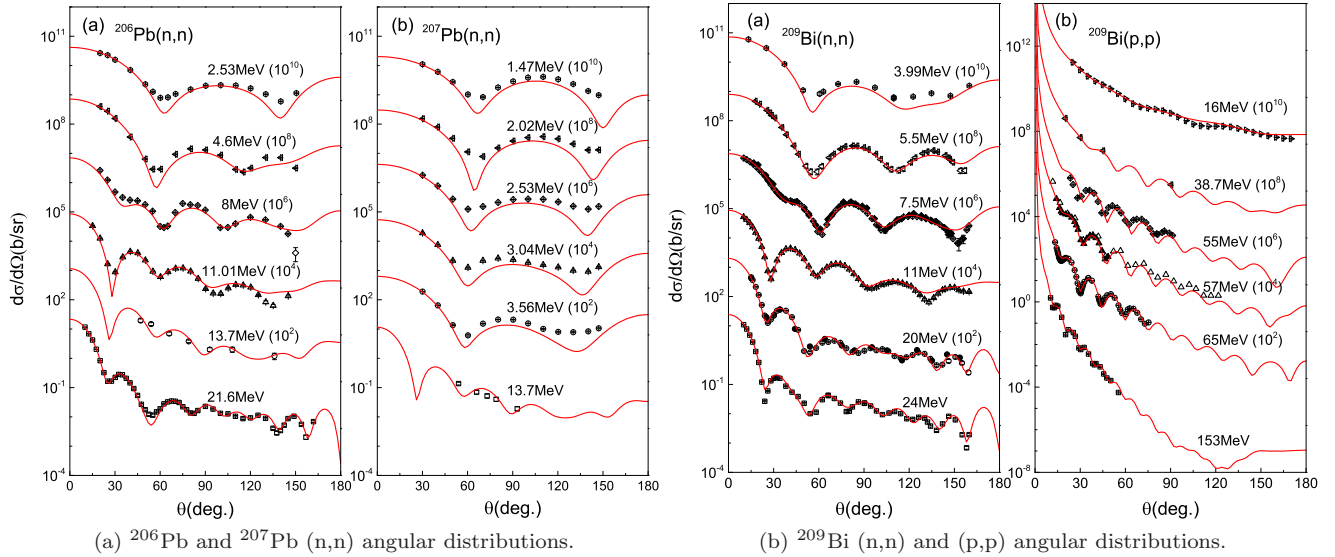
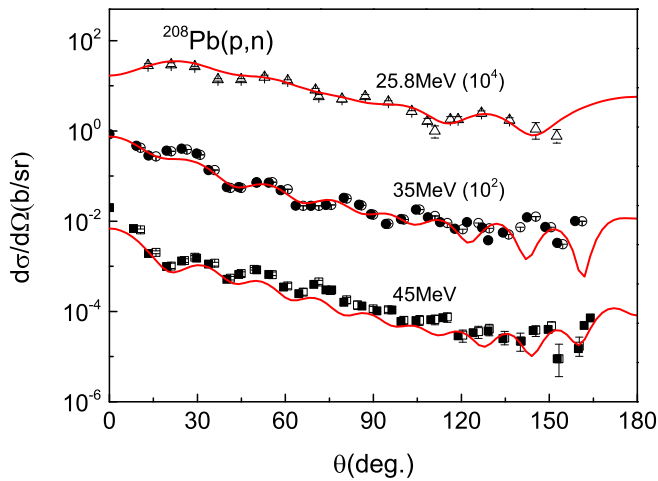
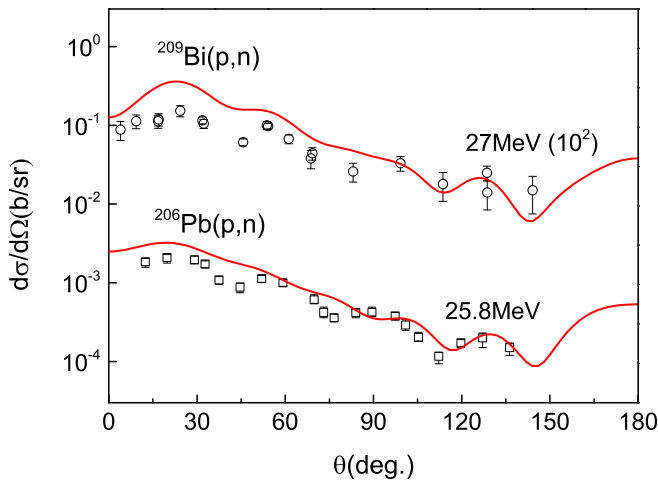


FIG. 6. Comparison of neutron and proton elastic scattering angular distributions with measurements at different incident nucleon energies.

^{207}Pb , and ^{209}Bi for different incident nucleon energies. Results for ^{208}Pb are similar to those presented in Ref. [11] and are not shown in this paper. The results for both neutron and proton elastic scattering describe the experimental data rather well over the entire energy and angular range. Slight underestimation of data below

5 MeV of neutron incident energy is probably associated with the missing compound-elastic contribution.

Figure 7 shows the calculated quasi-elastic (p,n) angular distribution for scattering on ^{206}Pb , ^{208}Pb and ^{209}Bi targets. Good agreement with data is achieved showing the Lane consistency of the derived DOMP, *i.e.*, the same

(a) ^{208}Pb quasi-elastic (pn) scattering angular distributions.(b) ^{206}Pb and ^{209}Bi quasi-elastic (pn) scattering angular distributions.FIG. 7. Calculated angular distributions of the quasi-elastic (pn) scattering on ^{206}Pb , ^{208}Pb and ^{209}Bi targets.

potential describes both neutron and proton scattering indistinctly, including the quasi-elastic (p,n) scattering that mainly is defined by the isovector potential.

IV. CONCLUSIONS

In order to improve the description of the nucleon scattering data and the bound-state energies using a dispersive potential, this work considered the non-locality of the real potential as suggested by Perey and Buck [17], and the impact of the large shell gap in magic nuclei on the definition of the imaginary potential [2, 23, 24]. The improved physical optical model potential that accurately describes scattering data for nucleon induced reactions on the double-magic target ^{208}Pb . The real part of the same DOMP, which corresponds to the shell potential, gives a good description of the bound-state data. Newly derived potential is also shown to give a good description of neutron and proton scattering on near-magic lead and Bi isotopes, which is very important for applications.

ACKNOWLEDGEMENT

This work is partly supported by Science Challenge Project, No. TZ2018001 and TZ2018005.

-
- [1] W. H. Dickhoff, and R. J. Charity, “Recent developments for the optical model of nuclei,” *Prog. in Part. Nucl. Phys.* **105**, 252–299 (2019).
 - [2] C. Mahaux, P. F. Bortignon, R. A. Broglia, and C. H. Dasso, “Dynamics of the shell model,” *Phys. Rep.* **120**, 1 (1985).
 - [3] C. Mahaux and R. Sartor, “Calculation of the shell-model potential from the optical-model potential,” *Phys. Rev. Lett.* **57**, 3015 (1986).
 - [4] E. Sh. Soukhovitskiĭ, R. Capote, J. M. Quesada, and S. Chiba, “Dispersive coupled-channel analysis of nucleon scattering from ^{232}Th up to 200 MeV,” *Phys. Rev.* **C67**, 067601 (2005).
 - [5] R. Capote, E. Sh. Soukhovitskiĭ, J. M. Quesada, and S. Chiba, “Is a global coupled-channel dispersive optical model potential for actinides feasible?,” *Phys. Rev.* **C72**, 064610 (2005).
 - [6] R. Capote, S. Chiba, E. Sh. Soukhovitskiĭ, J. M. Quesada, and E. Bauge, “A global dispersive coupled-channel optical model potential for actinides,” *J. of Nucl. Sc. Tech.* **45**, 333–340 (2008).
 - [7] R. Capote *et al.*, “RIPL–Reference Input Parameter Library for Calculation of Nuclear Reactions and Nuclear Data Evaluations,” *Nucl. Data Sheets* **110**, 3107–3214 (2009) (see www-nds.iaea.org/RIPL-3/).
 - [8] R. Li, W. Sun, E. Sh. Soukhovitskiĭ, J.M. Quesada, and R. Capote, “Dispersive coupled-channels optical-model potential with soft-rotator couplings for Cr, Fe, and Ni isotopes,” *Phys. Rev.* **C87**, 054611 (2013).
 - [9] E. Sh. Soukhovitskiĭ, R. Capote, J. M. Quesada, S. Chiba, and D. S. Martyanov, “Nucleon scattering on actinides using a dispersive optical model with extended couplings,” *Phys. Rev.* **C94**, 064605 (2016).
 - [10] W. Sun, J. Wang, E. Sh. Soukhovitskiĭ, R. Capote and J. M. Quesada, “Description of nucleon scattering on ^{208}Pb by a fully Lane-consistent dispersive spherical optical model potential,” *EPJ Web of Conferences* **146**, 12010 (2017).
 - [11] X. Zhao, W. Sun, E. Sh. Soukhovitskiĭ, D. S. Martyanov, J. M. Quesada, and R. Capote, “Analysis of neutron

- bound states of ^{208}Pb by a dispersive optical model potential”, *J. Phys. G.* **46**, 055103 (2019).
- [12] B. Morillon and P. Romain, “Dispersive and global spherical optical model with a local energy approximation for the scattering of neutrons by nuclei from 1 keV to 200 MeV,” *Phys. Rev.* **C70**, 014601 (2004).
- [13] B. Morillon and P. Romain, “Bound single-particle states for neutrons from a global spherical optical model,” *Phys. Rev.* **C74**, 014601 (2006).
- [14] C. H. Johnson, D. J. Horen, and C. Mahaux, “Unified description of the neutron- ^{208}Pb mean field between -20 and +165MeV from the dispersion relation constraint,” *Phys. Rev.* **C36**, 2252 (1987).
- [15] J. M. Quesada, R. Capote, A. Molina, M. Lozano, “Dispersion relations in the nuclear optical model,” *Comp. Phys. Commun.* **153**, 97–105 (2003).
- [16] J. M. Quesada, R. Capote, A. Molina, M. Lozano, J. Raynal, “Analytical expressions for the dispersive contributions to the nucleon-nucleus optical potential,” *Phys. Rev. C* **67**, 067601 (2003).
- [17] F. G. Perey and B. Buck, “A non-local potential model for the scattering of neutrons by nuclei,” *Nucl. Phys.* **32**, 353 (1962).
- [18] A. M. Lane, *Phys. Rev. Lett.* **8**, 171 (1962).
- [19] A. M. Lane, *Nucl. Phys.* **35**, 676 (1962).
- [20] G. E. Brown and M. Rho, “The giant Gamow-Teller resonance,” *Nucl. Phys.* **A372**, 397 (1981).
- [21] J.P. Delaroche, Y. Wang, and J. Rapaport, “Neutron- ^{90}Zr mean field from a dispersive optical model analysis,” *Phys. Rev.* **C39**, 391 (1989).
- [22] A. J. Koning and J. P. Delaroche, “Local and global nucleon optical models from 1 keV to 200 MeV,” *Nucl. Phys.* **A713**, 231 (2003).
- [23] C. Mahaux and R. Sartor, “Single-particle motion in nuclei,” *Advances in Nuclear Physics*, volume 20 (edited by J.W. Negele and E. Vogt). Plenum, New York (1991).
- [24] A. Molina, R. Capote, J.M. Quesada, M. Lozano, “Dispersive spherical optical model of neutron scattering from 27 Al up to 250 MeV,” *Phys. Rev.* **C65**, 034616 (2002).
- [25] C. Mahaux and R. Sartor, “Dispersion relation approach to the mean field and spectral functions of nucleons in ^{40}Ca ,” *Nucl. Phys.* **A528**, 253 (1991).
- [26] E. Sh. Soukhovitskiĭ, S. Chiba, O. Iwamoto, K. Shibata, T. Fukahori, and G. B. Morogovskii, “Programs OPTMAN and SHEMMAN Version 8,” Technical Report **JAERI-Data/Code 2005-002** (Japan Atomic Energy Research Institute, 2005).
- [27] E. Sh. Soukhovitskiĭ, G. B. Morogovskii, S. Chiba, O. Iwamoto, and T. Fukahori, “Physics and Numerical Methods of OPTMAN: A Coupled-channels Method Based on Soft-rotator Model for a Description of Collective Nuclear Structure and Excitation,” Technical Report **JAERI-Data/Code 2004-002** (Japan Atomic Energy Research Institute, 2004).
- [28] E. Sh. Soukhovitskiĭ, S. Chiba, R. Capote, J. M. Quesada, O. Iwamoto, K. Shibata, T. Fukahori, and G. B. Morogovskii, “Supplement to OPTMAN code, manual version 10,” Technical Report **JAERI-Data/Code 2008-025** (Japan Atomic Energy Research Institute, 2008).
- [29] J. M. Quesada, R. Capote, E.Sh. Soukhovitskiĭ, S. Chiba, Approximate Lane consistency of the dispersive coupled-channels potential for actinides, *Phys. Rev.* **C76**, 057602 (2007).
- [30] E. Sh. Sukhovitskiĭ, Y.-O. Lee, J. Chang, S. Chiba, and O. Iwamoto, “Nucleon interaction with ^{58}Ni up to 150 MeV studied in the coupled-channels approach based on the soft-rotator nuclear structure model,” *Phys. Rev.* **C62**, 044605 (2000).
- [31] EXchange FORmat database (EXFOR) is maintained by the Network of Nuclear Reaction Data Centers (see www-nds.iaea.org/nrdc/). Data available online (e.g., at www-nds.iaea.org/exfor/).
- [32] J. A. Harvey, Data available online at [31], 1999.
- [33] D. G. Foster Jr., D. W. Glasgow, “Neutron Total Cross Sections, 2.5-15MeV. I. Experimental,” *Phys. Rev.* **C3**, 576 (1971).
- [34] R. E. Shamu et al., “Neutron Total Cross Sections of ^{208}Pb , ^{232}Th , and ^{238}U from 5 to 150 MeV,” Lawrence Berkeley National Lab Report **LBL-11118**, 128(1980).
- [35] R. W. Finlay et al., “Neutron total cross sections at intermediate energies,” *Phys. Rev.* **C47**, 237 (1993).
- [36] J. A. Farrell *et al.*, “A possible ‘doorway’ state in ^{209}Pb and ^{208}Pb ,” *Phys. Lett.* **17**, 286 (1965).
- [37] S. F. Hicks *et al.*, “Neutron scattering cross sections for $^{204,206}\text{Pb}$ and neutron and proton amplitudes of E2 and E3 excitations,” *Phys. Rev.* **C49**, 103 (1994).
- [38] B. A. Benetskiy *et al.*, “Nuclear radii for some isotopes derived from total from total neutron cross-sections, *All Union Conference on Neutron Physics*, Kiev, 18-22 Apr, 2:47 (1977).
- [39] D. J. Horen, J. A. Harvey and N. W. Hill, “Doorway states in s-, p-, and d-wave entrance channels in $^{207}\text{Pb}+n$ reaction,” *Phys. Rev.* **C18**, 722 (1978).
- [40] J. L. Fowler and E. C. Campbell, “Total Neutron Cross Section of Pb^{208} ,” *Phys. Rev.* **127**, 2192 (1962).
- [41] G. D. Kim et al., “Measurement of Fast Neutron Total Cross Sections on ^{nat}Ta and ^{nat}Bi in the MeV Energy Range,” *J. Korean Phys. Soc.* **59**, 2233 (2011).
- [42] P. T. Guenther, A. B. Smith and J. F. Whalen, “Fast-neutron cross sections of elemental bismuth,” *Nucl. Sci. Eng.* **75**, 69 (1980).
- [43] T. W. Bonner et al., “Scattering of Fast Neutrons in Pb and Ag,” *Phys. Rev.* **97**, 985 (1955).
- [44] M. J. Martin, “Nuclear Data Sheets for A=208,” *Nucl. Data Sheets* **108**, 1583 (2007).
- [45] J. Chen and F.G. Kondev, “Nuclear Data Sheets for A=209,” *Nucl. Data Sheets* **126**, 373 (2015).